CAD scheme to detect hemorrhages and exudates in ocular fundus images

Yuji Hatanaka[*a], Toshiaki Nakagawa[b], Yoshinori Hayashi[b, c], Yutaka Mizukusa[d], Akihiro Fujita[d], Masakatsu Kakogawa[c], Kazuhide Kawase[e], Takeshi Hara[b], Hiroshi Fujita[b]
[a] Dept. of Electronic Control Engineering, Gifu National College of Technology, 2236-2 Kamimakuwa, Motosu-shi, Gifu 501-0495, Japan
[b] Dept. of Intelligent Image Information, Division of Regeneration and Advanced Med. Science, Graduate School of Medicine, Gifu University, 1-1 Yanagido, Gifu-shi, Gifu 501-1194, Japan
[c] Tak Co. Ltd., 4-32-12 Kono, Ogaki-shi, Gifu 503-0803, Japan
[d] Kowa Company Ltd., 1-3-1 Shinmiyakoda, Hamamatsu-shi, Shizuoka 431-2103, Japan
[e] Dept. of Ophthalmology, Ogaki Municipal Hospital, 4-86 Minaminokawa-cho, Ogaki-shi, Gifu 503-8502, Japan

ABSTRACT

This paper describes a method for detecting hemorrhages and exudates in ocular fundus images. The detection of hemorrhages and exudates is important in order to diagnose diabetic retinopathy. Diabetic retinopathy is one of the most significant factors contributing to blindness, and early detection and treatment are important. In this study, hemorrhages and exudates were automatically detected in fundus images without using fluorescein angiograms. Subsequently, the blood vessel regions incorrectly detected as hemorrhages were eliminated by first examining the structure of the blood vessels and then evaluating the length-to-width ratio. Finally, the false positives were eliminated by checking the following features extracted from candidate images: the number of pixels, contrast, 13 features calculated from the co-occurrence matrix, two features based on gray-level difference statistics, and a feature calculated from the extrema method. The sensitivity of detecting hemorrhages in the fundus images was 85% and that of detecting exudates was 77%. Our fully automated scheme could accurately detect hemorrhages and exudates.

Keywords: feature extraction, fundus image, detection, diabetic retinopathy

1. INTRODUCTION

The number of patients with adult diseases such as diabetes and hypertension is currently increasing in Japan. To prevent or detect these diseases at early stages, ophthalmologists rely on examining the fundus images obtained from over forty-years-old patients aged over 40 years during total health examinations or mass screenings. Diabetic retinopathy is a complication associated with diabetes, and there is a high probability that diabetic patients will develop this condition within 10 years from the onset of diabetes. Furthermore, diabetic retinopathy is the biggest cause of blindness. In Japan, there are approximately 7.4 million patients with diabetes and approximately 16.2 million patients who may have diabetes [1]. Approximately 40% of diabetic patients are thought to suffer from diabetic retinopathy. This disease can be prevented from developing into blindness if it is treated at an early stage. However, approximately 3,000 people are recorded to have lost their vision after the onset of diabetic retinopathy. The fundus photographs or images obtained by the fundus camera are used to diagnose diabetic retinopathy. Japanese ophthalmologists usually examine the presence of hemorrhages and exudates in order to diagnose diabetic retinopathy. Here, we use the term "hemorrhages" to include hemorrhages, microaneurysms, and neovascularizations and the term "exudates" to include both hard and soft exudates.

Recently, many studies on the use of fundus images in detecting diabetic retinopathy have been reported [2–9]. Niemeijer et al. proposed a method for detecting microaneurysms in fluorescein angiograms [2–4]. Their method

*hatanaka@gifu-nct.ac.jp; phone 81 58 320 1384; fax 81 58 320 1263; gifu-nct.ac.jp

Medical Imaging 2007: Computer-Aided Diagnosis, edited by Maryellen L. Giger, Nico Karssemeijer,
Proc. of SPIE Vol. 6514, 65142M, (2007) · 1605-7422/07/$18 · doi: 10.1117/12.708367

comprised two steps. Firstly, microaneurysms were detected by using a morphological filter. The false positives were then eliminated by analyzing the features. Serrano et al. proposed a method for detecting microaneurysms by the region growing technique in order to analyze fluorescein angiograms [5]. Generally, the methods to detect microaneurysms use fundus images enhanced by contrast medium.

The contrast observed in an image of microaneurysm is very low; therefore, ophthalmologists often detect microaneurysms by using fluorescein angiograms. However, it is difficult to use fluorescein as a contrast medium for diagnosing all the medical examinees subjected to mass screening; therefore, we aim to develop an automatic system for detecting hemorrhages and exudates in the fundus images without using fluorescein angiograms.

Walter et al. presented a method for the detection of exudates [6]. Their method uses a morphological filter and watershed transformation. Usher et al. presented a method for detecting hemorrhages, microaneurysms, and exudates [7, 8]. The region growing method used by them segmented the abnormal and retinal regions. Nagayoshi et al. presented a method that included two additional processes to this method [9]. One of these was the normalization of color pixel values, and the other was the use of color pixel values for blood vessels. Moreover, the previous method had the drawback of a long operation time of approximately 43 s per image [9]. In this study, we propose a method for detecting the abnormalities faster than the previous methods.

2. METHODS

2.1 Overall scheme

The flowchart of our overall detection scheme, including the steps developed by us, is shown in Fig.1. It consists of the following eight stages: (1) image digitization, (2) pre-processing, (3) extraction of optic nerve head, (4) detection of hemorrhage candidates, (5) elimination of false positives in blood vessels, (6) elimination of funicular shaped false positives, (7) detection of exudates candidates, and (8) elimination of false positives by feature analysis. Further details are described as follows.

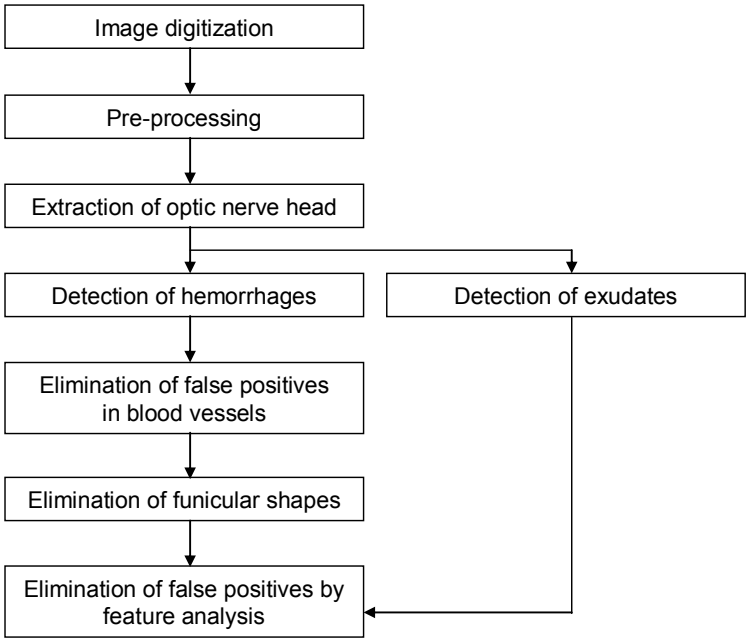

Figure 1 Flowchart for detecting hemorrhages and exudates in fundus images.

2.2 Image digitization and pre-processing of fundus images

We used the analog fundus photographs (45 or 50 degree field) captured on 35-mm positive films, as shown in Fig. 2 (a). The fundus images were digitized by an EPSON ES2000, a flatbed-type scanner with a transmissive unit. The

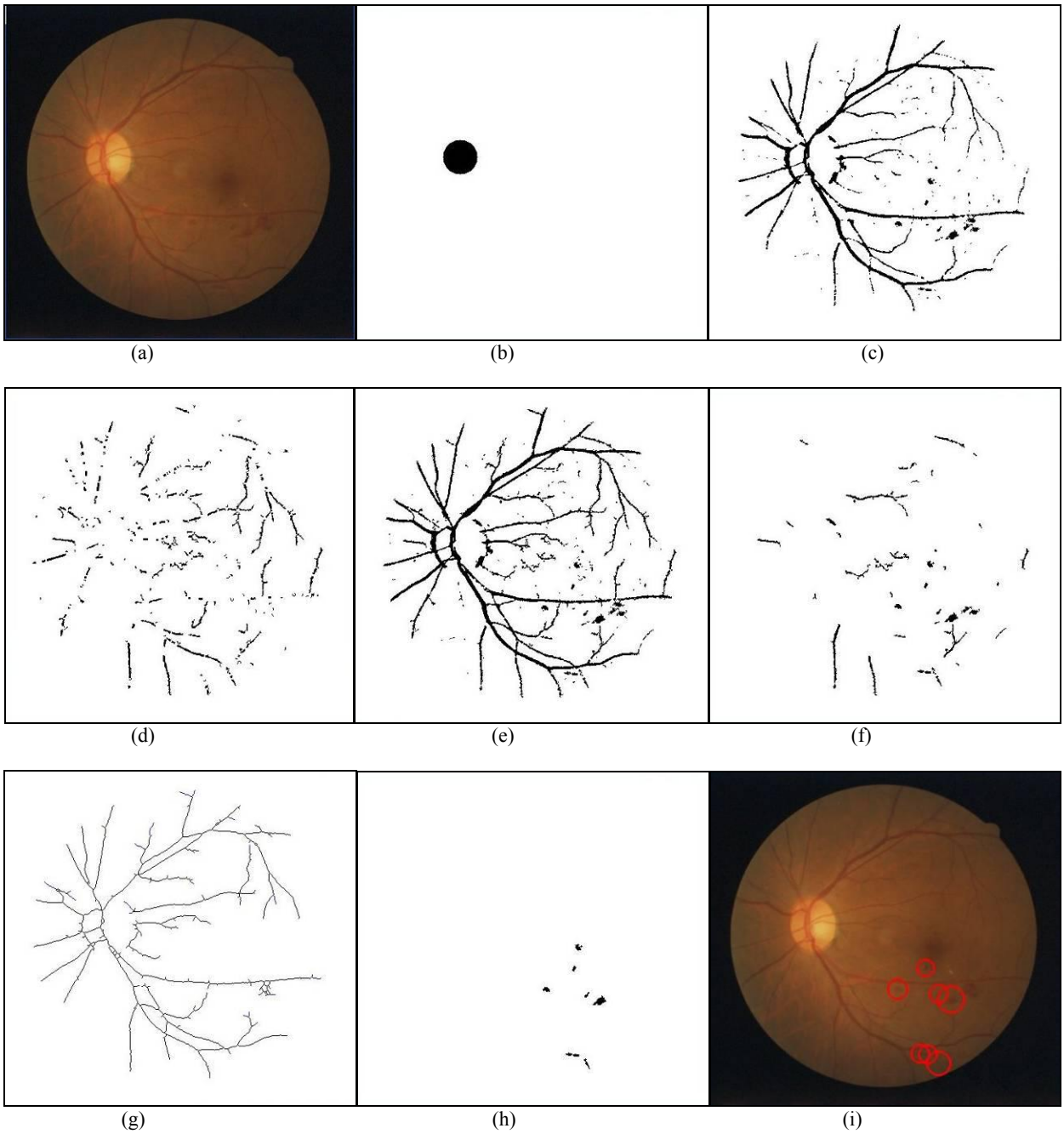

Figure 2 Illustration of the hemorrhage detection processes. (a) Input image. (b) Detected optic nerve head. (c) Roughly detected hemorrhages and blood vessels. (d) In detail detected hemorrhages and blood vessels. (e) Combination of (c) and (d). (f) Candidates connecting blood vessels and candidate with large areas were eliminated. (g) Centerlines of blood vessels were detected by a thinning technique. (h) False positives on the blood vessels were eliminated. (i) Final image of hemorrhage detection.

digitized 24-bit color images were represented by an array of 1,600 × 1,600 pixels in the bitmap format. Subsequently, the scale of the matrix was first reduced to the VGA size (width 640 pixels) by obtaining detailed subsamples from the

original image data to improve processing efficiency.

Next, the color images were converted to grayscale ones by selecting only the green component, thus achieving a clearer contrast as compared to the original ones, which include all the color components. The hemorrhages and exudates were then detected in these images. Finally, the brightness of the image was enhanced by using a method to equalize the histograms, and the noise was eliminated by a smoothing process.

2.3 Extraction of optic nerve head

After the optic nerve head was highlighted with a greater brightness than that used for highlighting other tissues, it was investigated by the p-tile technique. The shape of the detected region was approximated by a circle. Figure 2 (b) shows the image of the detected optic nerve head.

2.4 Detection of hemorrhage candidates

The pixel values of hemorrhages are lower than those of other regions; therefore, the hemorrhages were detected by performing finite difference calculations along with smoothing. This method was carried out in two steps: the rough and detailed detection processes. Firstly, the fundus images were smoothed by using a mask of 27 × 3 pixels. Next, the difference in pixel values between two smoothed images was calculated. Subsequently, the hemorrhage and blood vessel candidates were segmented by the thresholding technique. Figure 2 (c) shows an image of the roughly detected vessels. As shown in this image, the end of thin vessels was not detected. Therefore, the end of the vessels was detected by using a similar method that uses two types of images smoothed by using a mask of 9 × 3 pixels. Figure 2 (d) shows an image of the detailed parts of the vessels. By combining both types of techniques for the detection of hemorrhages and vessels, we could detect the all the blood vessels from the optic nerve head till the end of the vessels. Figure 2 (e) shows an image of the end of the vessels. Finally, the vessel candidates connected to the optic nerve head were eliminated, and the vessel candidates with large or very small areas were eliminated. Figure 2 (f) shows the resulting image.

2.5 Elimination of incorrectly detected vessels

The retinal vessel images include those reflected from the arterial wall, and the fundus images were obscured due to cataract. Therefore, it was difficult to detect all the vessels till the end by using the method proposed in section 2.3. We can resolve such difficulties by changing the threshold value proposed in section 2.3. However, the hemorrhage candidates were connected to the vessel candidates. Therefore, our method could not separate the connected candidates into hemorrhage and vessel candidates. The measures taken to resolve this problem are described as follows.

Firstly, the threshold value was selected in a manner that the vessels could be continuously detected. The centerlines of the vessels were extracted by using a thinning technique, as shown in Fig. 2 (g). Subsequently, the centerlines with large areas were extracted such that hemorrhage candidates could not be extracted. Finally, the vessels extracted on the centerlines were eliminated in order to avoid the vessels from being incorrectly detected. Figure 2 (f) shows the resulting image.

2.6 Elimination of funicular shapes

Since not all false positives on the vessels were eliminated by the method proposed in section 2.5, the remaining false positives were eliminated by evaluating the length-to-width ratio. The value of this ratio was small when the candidate was incorrectly detected as a vessel. The details of the evaluation are described as follows, and the illustration is shown in Fig. 3.

Firstly, the minimum rectangular region that surrounds the candidates was determined. The angle of the hemorrhage candidate was then determined by calculating the moment in order that the *X*- and *Y*-axes could be determined by using the obtained angle. Subsequently, binarized images were projected on the *X*- and *Y*-axes. By examining each of the projected images, the positions *Xa*, *Xb*, *Ya*, and *Yb* were determined. In this way, we could specify the black and white regions. Finally, we could determine the length-to-width ratio, denoted by *LW*, using the following equation:

$$LW = \frac{\min(|X_a - X_b|, |Y_a - Y_b|)}{\max(|X_a - X_b|, |Y_a - Y_b|)} \tag{1}$$

where $\min(|X_a - X_b|, |Y_a - Y_b|)$ is the mean value of the width, and $\max(|X_a - X_b|, |Y_a - Y_b|)$ is the mean value of the length.

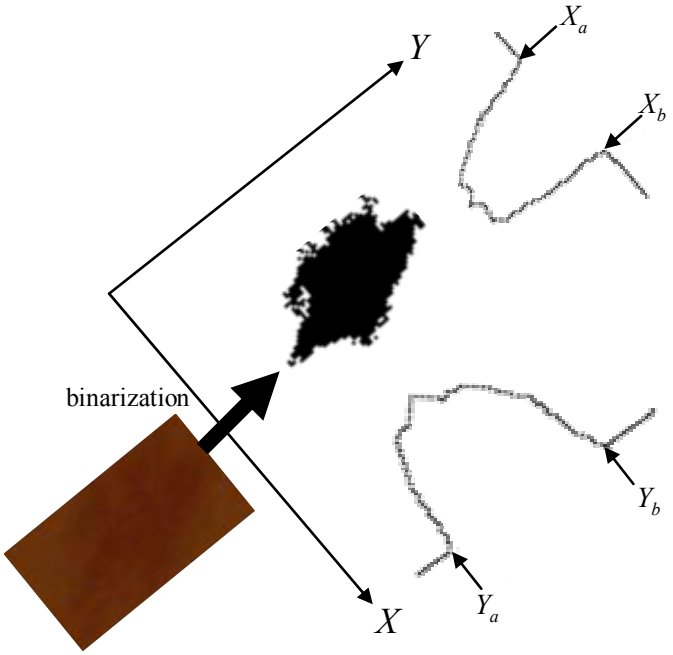

Figure 3 Feature extraction by evaluating the length-to-width ratio and the minimum width of a candidate, which are determined from the binarized hemorrhage image.

2.7 Detection of exudate candidates

The pixel values of exudates are brighter than those of other regions. Therefore, the exudates were detected by the same method as that used for hemorrhage detection. Firstly, the fundus images were smoothed by using a mask of 37 × 3 pixels. Then, the difference in the pixel values between two smoothed images, namely, the rough and detailed images, was calculated. Subsequently, the exudate candidates were segmented by the thresholding technique. Figure 4 (b) shows an image of the detected exudate candidates. Finally, the exudate candidates with a large area and those with very small areas were eliminated. Figure 4 (c) shows an image where the exudate candidates with a large area have been eliminated.

2.8 Elimination of false positives by feature analysis

The minimum rectangular region that surrounds the hemorrhage and exudate candidates extends beyond five pixels in each direction along the *X*- and *Y*-axes. Next, the average pixel values inside and outside the candidate region were calculated. Further, the contrast was determined by evaluating the ratio between the two average values. Figure 4 (d) shows an image obtained after the exudate false positives were eliminated based on the contrast.

Furthermore, we extracted the following features from the rectangle regions: 13 features calculated from the co-occurrence matrix [10], two features based on gray-level difference statistics [11], and one feature determined by the extrema method [12]. The 13 features were angular second moment, contrast, correlation, sum of square, inverse difference moment, sum average, sum variance, sum entropy, entropy, difference variance, difference entropy, and two kinds of information measurements for correlation. The two features based on gray-level difference statistics were angular second moment and mean. The minimum rectangular region that surrounds the candidates was determined. These features were calculated on the rectangular regions in the three grey level images, which comprised red, green, and blue bit images. Finally, the false positives were eliminated by a rule-base method. Fig. 2 (i) is an image obtained after hemorrhage detection; Fig. 4 (e), that obtained exudate after detection.

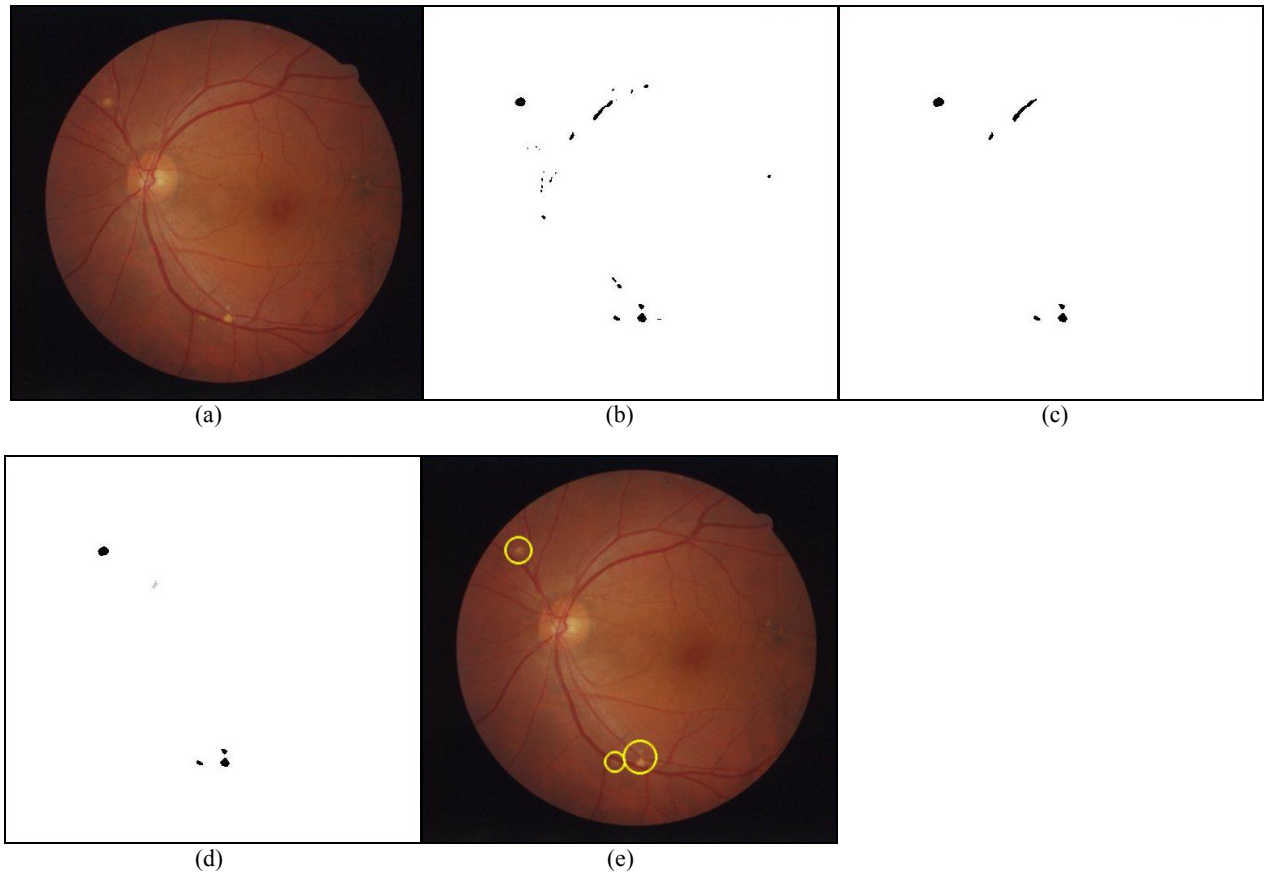

Figure 4 Illustration of the exudate detection process: (a) Input image. (b) Detected exudates. (c) Exudate candidates in image (b) with large areas were eliminated. (d) False positives were eliminated based on contrast. (e) Final result of exudate detection.

3. RESULTS AND DISCUSSION

To evaluate our method of detecting hemorrhages, we examined 113 fundus images, among which hemorrhages were detected in 26 images, and no abnormal cases were detected in the remaining 87 images. By using our scheme, we succeeded in obtaining satisfactory results with a sensitivity of 85% when the specificity was 21%. Our scheme could not detect four abnormal images. Three out of the four images included one image of a hemorrhage connected to the blood vessels and two images of hemorrhages identified as neovascular glaucomas. Since neovascularization is caused by ingravescence of diabetic retinopathy, the neovascular glaucomas do not have to be detected using a CAD during mass screening. Moreover, it was observed that one hemorrhage surrounds the exudates. Consequently, although our scheme could detect such exudates, it could not detect such a hemorrhage. Figure 5 shows a hemorrhage surrounding the exudates. Therefore, it can be said that our scheme could detect almost all cases of isolated hemorrhages. However, since the parameter of hemorrhage detection was selected such that microaneurysms could be detected, our scheme erroneously detected noise as a hemorrhage candidate. When the parameter of hemorrhage detection was selected such that the microaneurysms were not be detected, the specificity increased to 73%.

To evaluate our method for detecting exudates, we examined 109 fundus images, among which exudates were detected in 13 images, and no abnormal cases were detected in the remaining 96 images. By using our scheme, we succeeded in obtaining satisfactory results with a sensitivity of 77% when the specificity was 83%. Our scheme could not detect three abnormal images. In two of these images, the exudates were bright. Since the exudates in one image

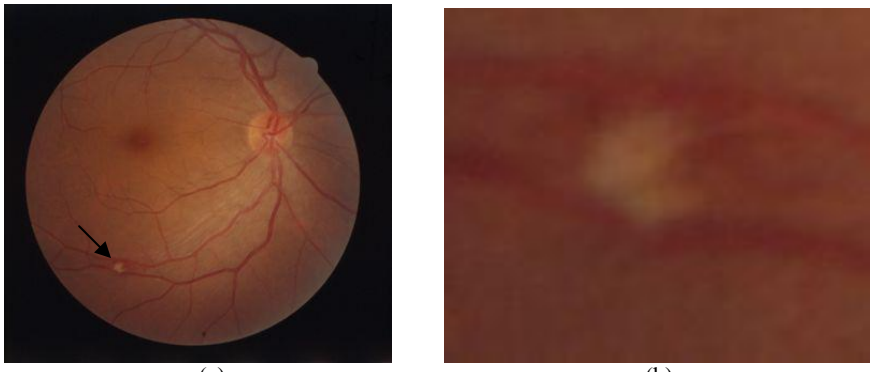

(a) (b)

Fig. 5. Hemorrhage surrounding the exudates. (a) A fundus image including a hemorrhage with exudates. A black arrow indicates a hemorrhage. (b) The enlarged image of the region indicated by the black arrow in (a).

were present on the eyelash, the characteristics of the exudates were different from the general ones. By selecting the parameters appropriate for exudate detection, our scheme could detect these two exudates. However, as the number of false positives increased, we did not change the parameters. The other exudates existed in an unusual fundus image, which was yellower than the conventional fundus images.

To eliminate the incorrectly detected hemorrhages, we used 13 features calculated from the co-occurrence matrix for each of three kinds of gray bit images. The most valid feature was the inverse difference measured for the green bit image, which could eliminate 24% of the false positives. Further, the second valid feature was difference variance measured for the blue bit image, which could eliminate 15% of the false positives. The contrast in the hemorrhage and retinal regions in the blue bit image was lower than that for the red bit image. However, the features calculated from the co-occurrence matrix in the blue bit image were the most effective. Therefore, we used 39 features calculated from the co-occurrence matrix for the three kinds of gray-level images in order to eliminate false positives.

We used an AMD Athlon X2 4600+-mounted (2.4 GHz) computer with a 4-GB memory operating in the SUSE Linux 10.1 environment. Processing each image required approximately 2.6 s. There were testing fundus images on the network access server (NAS), and the file size per image was approximately 6 MB. Therefore, our scheme could detect hemorrhages and exudates in real time.

4. CONCLUSION

In this study, a new scheme for automatically detecting hemorrhages and their exudates is presented by using digitized ocular fundus images as an example. This scheme can be applied to the computer-aided diagnosis (CAD) system for diagnosing diseases detected in the eyes. The results of the preliminary testing showed a desirable consistency with those obtained from the proposed scheme. It was demonstrated that the algorithm detected abnormalities with higher accuracy and reliability. The result of the initial work on fundus images clarified that the efficiency and accuracy of diabetic retinopathy diagnosis was considerably improved. The results of this study will be sent to ophthalmologists for further evaluation. The efficiency and accuracy diagnosing of diabetic retinopathy was improved due to the detection of hemorrhages and exudates with a higher accuracy. The application of the proposed scheme to fundus images enhances the CAD system performance for detecting hemorrhages and exudates in the fundus images. Presently, we are focusing our efforts on improving the scheme in order to minimize the problems mentioned in the discussion section. In the future, the integrated analysis scheme will be further improved, and more clinical cases will be reported for evaluating its accuracy. The techniques employed in our system will help in improving diagnostic accuracy as well as in reducing the workload of ophthalmologists in the future.

ACKNOWLEDGMENTS

The authors thank T. Yamamoto, T. Uchida, M. Aoyama, A. Aoyama, N. Kajima, M. Okamoto, and H. Mutoh for their considerable contributions to this study. This work was supported in part by a grant for the "Knowledge Cluster Creation Project" from the Ministry of Education, Culture, Sports, Science and Technology, Japan.

REFERENCES

1. "Health and Welfare Statistics Association," *J. Health Welfare Stat*., **51**, 144–148, 2004.
2. M. Niemeijer, B. V. Ginneken, J. Staal, M. S. Suttorp-Schulten and M. D. Abramoff, "Automatic detection of red lesions in digital color fundus photographs," *IEEE Transactions on Medical Imaging*, **24 (5)**, 584–592, 2005.
3. A. J. Framea, P. E. Undrill, M. J. Cree, J. A. Olson, K. C. McHardy, P. F. Sharp and J. V. Forrester, "A comparison of computer-based classification methods applied to the detection of microaneurysms in ophthalmic fluorescein angiograms," *Computers in Biology and Medicine*, **28 (3)**, 225–238, 1998.
4. A. D. Fleming, S. Philip, K. A. Goatman, J. A. Olson and P. F. Sharp, "Automated microaneurysm detection using local contrast normalization and local vessel detection," *IEEE Transactions on Medical Imaging*, **25 (9)**, 1223–32, 2006.
5. C. Serrano, B. Acha, S. Revuelto, "2D adaptive filtering and region growing algorithm for the detection of microaneurysms in retinal angiograms," *Medical Imaging 2004: Image Processing, Proceedings of SPIE*, **5370**, 1924–1931, 2004.
6. T. Walter, J. C. Klein, P. Massin and A. Erginay, "A contribution of image processing to the diagnosis of diabetic retinopathy-detection of exudates in color fundus images of the human retina," *IEEE Transactions on Medical Imaging*, **21 (10)**, 1236–1243, 2002.
7. C. Sinthanayothin, J. F. Boyce, T. H. Williamson, H. L. Cook, E. Menshan, S. Lal and D. Usher, "Automated detection of diabetic retinopathy on digital fundus images," *Diabetic UK Diabetic Medicine*, **19 (1)**, 105–112, 2002.
8. D. Usher, M. Dumskyj, M. Himaga, T. H. Williamson, S. Nussey and J. F. Boyce, "Automated detection of Diabetic retinopathy in digital retinal images: a tool for diabetic retinopathy screening," *Diabetic UK Diabetic Medicine*, **21 (1)**, 84–90, 2004.
9. H. Nagayoshi, Y. Hiramatsu, T. Kagehiro, Y. Mizuno, M. Himaga, H. Sakou, S. Sato, H. Fukushima and S. Kato, "Detection of lesions from fundus images for diagnosis of diabetic retinopathy," *IEICE Technical Report*, **105 (64)**, 61–66, 2005.
10. R. M. Haralick, "Statistical and structural approaches to texture," *Proceedings of the IEEE*, **67 (5)**, 1979.
11. J. S. Weszka, C. R. Dyer and A. Rosenfeld, "A comparative study of texture measures for terrain classification," *IEEE Transactions on Systems, Man, and Cybernetics*, **SMC-6 (4)**, 269–285, 1976.
12. O. R. Mitchell, C. R. Myers and W. Boyne, "A max–min measure for image texture analysis," *IEEE Transactions on Computers*, **C-2 (4)**, 408–414, 1977.